Stochastic Geometry Analysis of User Mobility in RF/VLC Hybrid Networks

Rabe Arshad and Lutz Lampe

***Abstract*—The integration of visible light communication (VLC) with existing radio frequency (RF) networks has emerged as a new network architecture to meet the rapidly growing traffic demand. The resulting RF/VLC hybrid network structures offer capacity-per-area improvements due to the use of two technologies operating at different frequency bands and the relatively higher base station (BS) density. However, the reduced BS coverage footprints and the heterogeneous BS types result in challenges for user mobility such as frequent handovers and the need for suitable BS association policies. To help addressing these challenges, in this paper, we conduct a user mobility analysis for RF/VLC hybrid networks by deriving the user-to-BS association probabilities and handover rates. The analysis makes use of stochastic geometry and modelling BSs' locations via a Poisson point process (PPP). Since PPP modelling has not yet been well established for hybrid RF/VLC networks, we support the applicability of our approach by comparing the user mobility performance to those obtained for an actual deployment, a Matérn hard-core point process (MHCPP) based deployment, and a deterministic square lattice deployment of VLC luminaries. Furthermore, since the handover rates directly depend on the association policies, we consider two popular association policies. Our numerical results show that the PPP, the MHCPP, the square lattice, and the actual deployments have comparable performance in terms of handover rates regardless of the association policy, and they highlight the tradeoff between balancing network load and handover rates achieved by the association policies.**

***Index Terms*—Association probabilities, Handover rates, Hybrid networks, Radio frequency networks, Stochastic geometry, Visible light communication**

I. Introduction

Network densification realized via heterogeneous base station (BS) deployment has proved to be an effective solution to meet the ever growing traffic requirements in wireless networks [1]. As a part of an extreme densification phase, diverse types of small BSs are being deployed within the same geographical area to offload the traffic from the existing BSs [2]. In fact, new advancements are being made especially for indoor small BSs. For instance, equipment providers like Ericsson and Huawei have introduced digital distributed networks named Radio Dot and Lampsite, respectively, that redefine the concept of small BSs [3]. While these concepts are able to offload traffic from macro BSs, the congested radio frequency (RF) spectrum may not be able to accommodate the projected capacity demand. Considering that indoor environments hold around 80% of the overall mobile traffic [3], alternatives that complement RF solutions are desirable.

Visible light communication (VLC) provides the ability to increase BS density without affecting the RF spectrum. VLC uses light emitting diode (LED) luminaries to transmit data via intensity modulation at the transmitter and direct detection at the receiver side. With off-the-shelf LEDs, VLC data rates of 15.73 Gb/s have been demonstrated [4]. Along with such impressive rates, the use of VLC in optical base stations (OBSs) brings several other benefits including inherent security, cost-effectiveness in terms of reusing the existing LED luminaries, and immunity to electromagnetic interference [5]. On the other hand, a stand-alone VLC network based on existing luminaries is challenging, since irregular illumination requirements may create coverage holes. Thus, in future wireless networks, VLC is expected to complement existing RF networks (e.g., wireless fidelity) resulting in a hybrid RF/VLC network. Several studies including [6] and [7] are available in the literature that highlighted the rate gains achieved in RF/VLC hybrid networks. In fact, several case studies have also been conducted where OBSs were deployed in several places including schools and hospitals [8]. While the aforementioned studies motivated the integration of VLC into existing RF networks, there exist some other studies that focus on the challenges foreseen through this integration and added heterogeneity. For instance, the authors in [9] and [10] presented power efficient RF/VLC hybrid network paradigms where the total power consumption was minimized under defined quality of service constraints. The authors in [11] quantified the minimum spectrum and power requirements in RF to offer a certain per user rate coverage performance in a hybrid RF/VLC network setting. Furthermore, the authors in [12] optimized the intensities of RF and VLC BSs to minimize the area power consumption. The authors in [13] studied the energy efficiency maximization problem in an aggregated RF/VLC system. However, [6]–[13] did not discuss the user mobility challenges in RF/VLC hybrid networks.

While adding heterogeneous BSs to existing networks provides better coverage, per-user rate, and localization accuracy, the reduced per-BS coverage areas encourage mobile users to perform frequent handovers. Handover (HO) is a process involving a change in the user-to-BS association and is triggered depending upon pre-defined HO criteria. Moreover, the total number of HOs per unit time, i.e., the HO rate, depends on several factors including BS density, transmit power, and user velocity. While network heterogeneity helps achieving the desired capacity improvements, it generally causes an increase in the overall HO rates, which may deteriorate network key

This work was supported by the Natural Sciences and Engineering Research Council of Canada (NSERC).

Rabe Arshad and Lutz Lampe are with the Department of Electrical and Computer Engineering, University of British Columbia, Vancouver, BC V6T1Z4, Canada. Email: {rabearshad, lampe}@ece.ubc.ca.

performance indicators (KPIs) [14].

The negative effects of HOs on the network performance are mainly due to the HO associated communication delays when there is no application-data transmission between a user and the BS, signalling overhead, and power consumption at the BS and the user end. The amount of delay depends on the type of HO, i.e., horizontal or vertical, and the network architecture. For instance, the HO delay in Wi-Fi networks may reach up to 1 second [15]. The impact of HOs and the associated delays would become more prominent in RF/VLC hybrid networks. This is due to the much smaller coverage areas with possibly much higher density of OBSs. Similarly, the increased network densification would encourage users to send measurement reports to the network more often, which will add to the signalling overhead and will result in the increased power consumption both at the BS and the user end [16]. Hence, a thorough understanding of the effect of user mobility and HO strategies in RF/VLC hybrid systems as a function of BSs' intensity is required. This is the main motivation for us to study the user-to-BS association and HO rates in RF/VLC hybrid networks.

A. Related Work

The significance of network densification and the resulting HO rate problem has been addressed in the literature. For instance, the authors in [17] and [18] presented methods to reduce the number of unnecessary HOs in multi-tier indoor and outdoor RF networks, respectively. Several studies including [19]–[21] and [22]–[24] presented HO related algorithms to improve the user experience in RF only and VLC only networks, respectively. In the context of RF/VLC hybrid networks, the authors in [25] proposed a vertical HO scheme to reduce the HO signalling cost. Moreover, [26] studied load balancing by taking user mobility and HO signalling into account. The work in [26] was extended in [27] where the authors presented a dynamic load balancing algorithm to improve the user rate. However, the quantitative analysis of the impact of user mobility on the HO rates is still an open problem.

With regards to HO rate modelling, relatively few studies exist in the literature for RF only networks. For instance, [28] and [29] characterized HO rates in a Poisson point process (PPP) based single tier and multi-tier RF network, respectively. While [28], [29] used user trajectory based approach to characterize handover rates, the authors in [30], [31] used association based approach to calculate handover probability[1]. The model in [29] was extended in [36] for three-dimensional ultra-dense RF networks. It is worth mentioning that the existing HO models presented in the literature (i.e., [28]–[31], [36]) cannot directly be applied to VLC networks due to the involvement of the field-of-view (FOV) of VLC receivers. For VLC networks, the authors in [37] studied the impact of device rotation on the HO probability. However, [37] did not incorporate the impact of BS density on the HO rates and rather considered four BSs with the square lattice deployment. To the best of our knowledge, no study exists that characterizes the HO rates and presents the interplay between BSs intensity and HO rates as a function of receiver FOV in VLC only and RF/VLC hybrid networks.

For a general study on the impact of BS densification on the network performance, a random BS deployment is usually considered. This can be realized via stochastic geometry, which is a mathematical tool that helps modelling the randomness in BSs' locations through different point processes and captures the network performance in terms of spatial averages. Despite the existence of several point processes, abstracting the RF BSs' locations using a PPP has widely been adopted in the literature due to mathematical tractability and its predictive power for the performance of actual wireless networks [29], [38]. In the context of VLC networks, it is shown in [39] that the PPP based modeling is the most appropriate and tractable for the outage performance analysis in an indoor environment with multiple optical BSs. Recently, PPP modeling has also been applied to RF/VLC hybrid networks to study coverage and rate performance [40]. However, a stochastic geometry aided user mobility analysis and a performance comparison with respect to an actual deployment scenario are yet to be conducted for RF/VLC hybrid networks.

B. Paper Contributions

The main contributions of this paper are summarized as follows.

- We present analytical expressions for the association probabilities and HO rates in RF/VLC hybrid networks. The analytical framework is necessary as it helps understanding the impact of different network parameters on the network performance, which is cumbersome otherwise. For the mathematical analysis, we model the BSs' locations via a PPP and use stochastic geometry to capture the interplay between HO rates and network parameters (e.g., BS intensity). Analytical approximations are validated via Monte-Carlo simulations. In order to conduct a more comprehensive user mobility analysis, we compute the HO rates based on two user-to-BS association policies: i) Opportunistic VLC, which allows the users to connect to the OBSs as long as they lie in the OBS coverage area and ii) Received signal strength (RSS), where the user associates to the tier that offers the highest received signal power.
- The PPP assumption for abstracting the BSs' locations is necessary to mathematically characterize the association probabilities and the HO rates. However, it has not been well understood yet if this is a realistic approximation for the deployment model of OBSs. For example, considering the desired reuse of existing luminaries by VLC, a square lattice deployment or a hard-core point process (HCPP) seem to better approximate the actual indoor lighting arrangement in many places such as office buildings. At the same time, the wiring complexities and uncertain

[1]Handover rate is used to determine the ping pong handover rate, handover failure rate, quantify the mobility effect into the signalling overhead, power consumption, and average throughput experienced by the user [16], [32], [33]. Handover probability is used to investigate the handover drop probability and unnecessary handover probability [34]. Under certain conditions (e.g. low user velocity), the handover rate is equal to the handover probability [35].

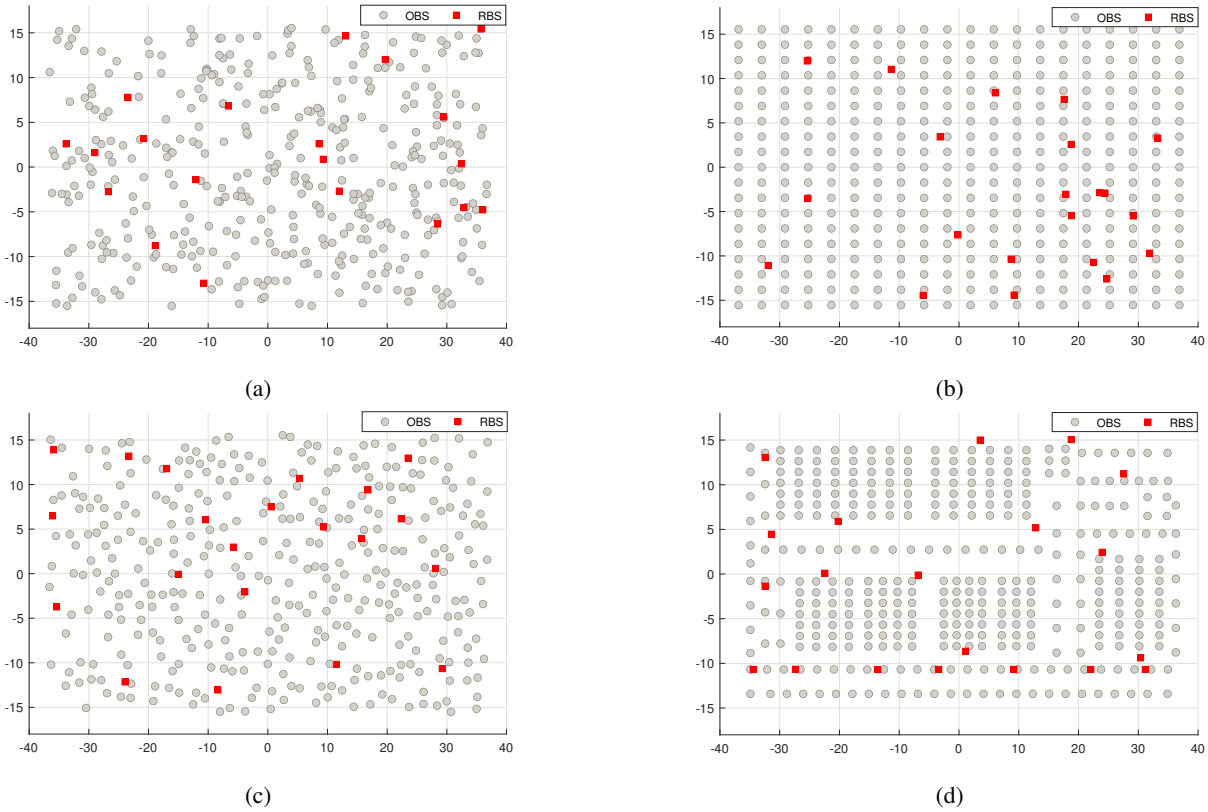

Fig. 1: A two tier RF and optical BS network in a 74 m $\times$ 31 m indoor area according to four deployment models: (a) PPP, (b) square lattice deployment for VLC and PPP for RF, (c) Matérn HCPP with $d_{\mathrm{v}} = 1.3$ m, $d_{\mathrm{r}} = 5$ m, (d) an actual deployment in a university building. RF and optical BSs are represented by red squares and gray circles, respectively.

lighting requirements in some areas may call for a more random-like deployment [41]. Thus, in addition to the analytical modelling via PPP, we simulate the BSs' locations according to a square lattice, Matérn HCPP (MHCPP), and an actual placement of luminaries in a university building. In the square lattice deployment, VLC BSs follow the square lattice pattern while RF BSs (RBSs) still follow the PPP deployment. In MHCPP, the BSs are not allowed to be closer by a certain distance d, which mimics a practical deployment setting. These scenarios are illustrated in Fig. 1. We compare the association probabilities and HO rates for the different deployment cases to shed light on the applicability of PPP for RF/VLC hybrid networks.

- Using the developed mathematical model, we present the impact of an VLC centric element (receiver FOV) on the association probabilities and inter/intra tier HO rates under the considered BSs' deployment models. We also highlight an optimal FOV range and BSs' heights where the HO rates tend to be constant. Moreover, via simulation results from the actual deployment scenario, it is shown that the developed analytical model captures the user mobility performance in RF/VLC hybrid networks.

One of the major challenges in this study lies in the complexity of the analytical modeling, due to the involvement of different path loss models, BSs' heights, and receiver FOV. Hence, the presented solutions for the handover rates are thus not closed form but require additional one-dimensional integration over some parameters.

C. Paper Organization and Notations

The rest of the paper is organized as follows. The system model is presented in Section II. The association probabilities and the service distance distributions are derived in Section III. The analytical framework for the HO rates is presented in Section IV. Finally, the simulation setup and the performance comparison among different deployment strategies are discussed in the Section V followed by the conclusion in Section VI. The mathematical notations used in the paper are summarized in Table I.

II. Hybrid RF/VLC System Model

In this section, we describe the system model for the RF/VLC hybrid network.

A. Network Model

As mentioned in the introduction, the BSs' locations in the two tier RF/VLC hybrid network are modeled via four different deployment models, which are illustrated in Fig. 1. In the PPP deployment, the number of BSs inside any bounded region is a Poisson random variable and each BS acquires a random location within the defined area. In a two tier RF/VLC hybrid network, BSs belonging to each tier $k \in \{\mathrm{r},\mathrm{v}\}$ are

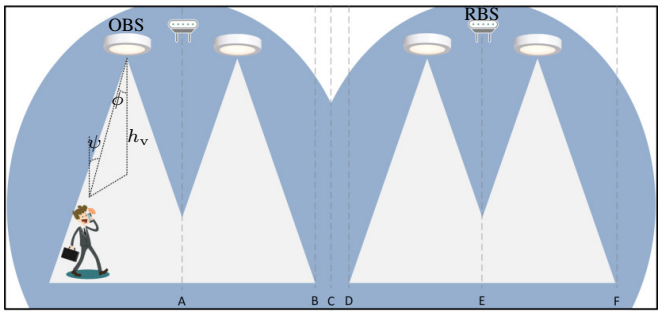

Fig. 2: A two tier RF/VLC hybrid network with the RBS and OBS coverage areas represented by blue and white colors, respectively. For a mobile user walking to the right, the intra and inter-tier HOs are represented by {A, C, E} and {B, D, F}, respectively.

TABLE I: Mathematical Notations

Notation	Description
λ_k	BS intensity of k^{th} tier
P_{r}	Transmit power of RBSs
P_{opt}	Optical transmit power of OBSs
P_{elec}	Electrical transmit power of OBSs
B_k	Bias factor of k^{th} tier
h_k	Height of k^{th} tier BS
Z_k	Euclidean distance between the user and the nearest BS of k^{th} tier
R_k	Horizontal distance between the user and the nearest BS of k^{th} tier
n_{c}	Optical-to-electrical conversion ratio
η	Path-loss exponent
ψ	Angle of incidence from nearest OBS to user
H_{ij}	Handover rate from tier i to j
A_k	Probability of associating to the k^{th} tier BS
G	DC channel gain for VLC communication
ζ	Receiver field-of-view
B, C	RF Propagation model dependent constants

placed via a two-dimensional homogeneous PPP at height h_k, where "r" and "v" identify RBSs and OBSs, respectively. For the square lattice deployment, the VLC and RF BSs' locations follow a grid pattern and PPP, respectively, where the total numbers of BSs are obtained from the actual lighting and Wi-Fi BSs data in accordance with the actual deployment case. MHCPP deployment results from a dependent thinning applied to a homogeneous PPP and accounts for the fact that the inter-BS distance d_k should not be less than a certain threshold [42]. Finally, the actual deployment is obtained from the lighting and Wi-Fi BSs arrangements on a building floor at the University of British Columbia.

While we derive the mathematical expressions of HO rates for PPP, the HO rates in the square lattice, MHCPP, and the actual luminaries deployments are computed via simulations. For all deployment models, the RBSs and OBSs are located at the ceiling and are oriented vertically downward. Without loss of generality, we conduct our analysis on a test mobile user that follows a horizontal random waypoint mobility model with velocity v. It is assumed that the test user is equipped with both RF and VLC receivers. The VLC receiver uses a photo-detector that is assumed to face upward, i.e., toward the ceiling, which is in accordance with the recent studies [40], [43]. The impact of device rotation on the HO rate is out of scope of this paper and considered for future study.

The coverage areas of RBSs and OBSs can be visualized via a weighted Voronoi tessellation [44]. For illustrative purposes, Fig. 2 depicts the coverage areas of RBSs and OBSs and the HO regions. Depending upon the association policy, the test user performs an HO as soon as it enters the coverage area of the target BS. It is assumed that the requested HOs are always successful.

B. Channel Model

We adopt the WINNER channel model for RF communication because of its applicability for indoor environments [45]. The received power can be modeled as $P^{\text{RF}} = P_{\text{r}} X Z_{\text{r}}^{-\eta}$, where P_{r} is RBS transmit power, Z_{r} is the Euclidean distance between the user and the nearest RBS, η represents the free space path-loss exponent, and $X = 10^{-\frac{\gamma}{10}}$, $\gamma = B + C\log_{10}(f_{\text{c}}/5)$, f_{c} is the carrier frequency in GHz, and B and C are propagation model dependent constants. For the line-of-sight (LOS) scenario, $B = 46.3$ and $C = 20$ [45].

For the VLC communication, the received power can be modeled as $P^{\text{VLC}} = P_{\text{elec}} G^2 R_{\text{pd}}^2$, where P_{elec} represents the OBS electrical transmission power, G denotes the VLC channel gain, R_{pd} represents the responsivity of the photo-detector in the receiver [39]. As per [46], the average electrical and the optical power in direct current biased optical orthogonal frequency division multiplexing system are related by $P_{\text{elec}} = P_{\text{opt}}^2/n_{\text{c}}^2$, where n_{c} is the optical-to-electrical conversion ratio. Due to high intensity of OBSs, it is highly probable that there exists the LOS communication between the user and the OBS. Thus, the LOS direct current (DC) channel gain is used in the analysis, which is modeled via the Lambertian emission model and given as [47]

$$G = \begin{cases} \frac{(m+1)}{2\pi Z_{\text{v}}^2} A_{\text{pd}} \cos^m(\phi)\cos(\psi) G(\zeta) T(\zeta), & 0 \le \psi \le \zeta \\ 0, & \psi > \zeta \end{cases}, \quad (1)$$

where A_{pd} is the physical area of the receiver photo-detector, Z_{v} represents the Euclidean distance between the user and the nearest OBS, ϕ is the angle of radiance from the nearest OBS, ψ is the angle of incidence from nearest OBS to the user, ζ is the receiver FOV, and m is the order of Lambertian emission that can be calculated as $m = \ln(2)/\ln(\cos(\Phi_{1/2}))$. The half-power semi-angle $(\Phi_{1/2})$ represents the angle of radiance at which the transmitted optical power gets half when compared to the power at $\phi = 0$. $T(\zeta)$ is the gain of the optical filter at the receiver and $G(\zeta) = n^2/\sin^2(\zeta)$ is the gain of the non-imaging concentrator where n is the refractive index. As stated earlier, we assume that the user moves along the horizontal axis with the photo-detector facing upward. This implies that $\phi = \psi$. Using the fact that $\cos(\phi) = \cos(\psi) = \frac{h_{\text{v}}}{Z_{\text{v}}}$, G can be simplified to

$$G = \begin{cases} \frac{(m+1) A_{\text{pd}} G(\zeta) T(\zeta) h_{\text{v}}^{m+1}}{2\pi Z_{\text{v}}^{m+3}}, & 0 \le \psi \le \zeta \\ 0, & \psi > \zeta \end{cases}. \quad (2)$$

III. Association and Distance Analysis

Since a mobile user performs a HO at the point of intersection between the individual cell boundaries followed by the user-to-BS association changes, the HO rates directly depend on the association probabilities and the number of intersections between the user trajectory and the cell boundaries. Given a fixed user trajectory, a larger number of intersections per unit time will yield a higher HO rate. As we exploit stochastic geometry to obtain spatial averages of the performance metrics, it is important to characterize the service distance distributions so that the performance metrics can be averaged over all user locations. In this section, we develop the mathematical framework for the association probabilities and the service distance distributions that will be used for the characterization of HO rates in Section IV.

We adopt two of the most popular user-to-BS association policies, which are defined as follows.

1) Opportunistic VLC Association: The opportunistic VLC policy allows a user to access an OBS whenever possible and RF otherwise. If multiple OBSs are available, the user opts for the OBS providing the strongest signal, i.e., the nearest OBS. A similar association strategy was proposed in [48] and [49] where the downlink traffic in a hybrid RF/VLC network was completely handled by OBSs. The first motivation behind this policy is that a user might want to associate to the VLC BS provided that there exists a large disparity between the available data rates of RF and VLC. In such a case, the opportunistic VLC association policy mimics a rate based association. The second motivation is to offload data traffic from the RF spectrum whenever possible. The availability of VLC coverage in a particular region depends on the receiver's location and FOV. A user is within the VLC coverage if the angle of incidence from the target OBS to the user is less than the receiver FOV, i.e., $\psi \leq \zeta$.

2) RSS Association: The RSS based association policy allows a user to associate to the BS that offers the best received signal strength. This policy has been widely studied in the literature. For instance, under RSS policy, the authors studied the user-to-BS association probabilities in [38], [50] for RF and in [40] for RF/VLC hybrid networks. It is worth mentioning that [40] did not incorporate the heights of RF BSs into the mathematical analysis. While incorporating BSs' heights into the mathematical analysis is crucial due to its impact on the network performance [51], the resulting mathematical model is not straightforward.

A. Association Probabilities

We will now present the mathematical expressions for the association probabilities in RF/VLC hybrid networks under RSS and opportunistic VLC policies.

In the opportunistic VLC association policy, the user connects to the nearest OBS as long as it lies within the VLC coverage. This implies that the VLC association probability will be the probability $\mathbb{P}[\psi \leq \zeta]$, which is given by the following lemma.

Lemma 1 (Association probability with Opportunistic VLC policy):

Let R_{v} be the horizontal distance between the user and the projection of the closest OBS on the ground. Then the association probabilities under opportunistic VLC policy[2] are given by

$$A_{\mathrm{VLC}}^{(\mathrm{OPP})} = \mathbb{P}\big[\psi \leq \zeta\big] = \mathbb{P}\left[\tan^{-1}\left(\frac{R_{\mathrm{v}}}{h_{\mathrm{v}}}\right) \leq \zeta\right]$$
$$= \mathbb{P}[R_{\mathrm{v}} \leq h_{\mathrm{v}}\tan(\zeta)] = 1 - \mathrm{e}^{-\pi\lambda_{\mathrm{v}}h_{\mathrm{v}}^2\tan^2(\zeta)} \triangleq P_0 \quad (3)$$
$$A_{\mathrm{RF}}^{(\mathrm{OPP})} = \mathbb{P}\big[\psi > \zeta\big] = 1 - P_0. \quad (4)$$

From (3), it is observed that the VLC association probability does not depend on the OBS transmit power rather depends on the OBS intensity, OBS height, and receiver FOV. An increase in any of the three parameters will push more traffic toward VLC. In case of RSS association, the user associates to the BS that offers the highest biased received power. The respective association probabilities under RSS policy are given by the following lemma.

Lemma 2 (Association probabilities with RSS policy):

The RF and VLC association probabilities in a PPP based RF/VLC hybrid network with RSS association policy are given in (5) and (6), respectively, where

$$D = \left(\frac{4\pi^2 K B_{\mathrm{r}} P_{\mathrm{r}} h_{\mathrm{v}}^{-2(m+1)}}{B_{\mathrm{v}} P_{\mathrm{elec}} R_{\mathrm{pd}}^2 (m+1)^2 A_{\mathrm{pd}}^2 G^2(\zeta) T^2(\zeta)}\right)^{\frac{1}{\eta}}, \quad (7)$$

$$Q = \begin{cases} \min\left[\left(\frac{h_{\mathrm{r}}}{D}\right)^{\frac{1}{\alpha}}, h_{\mathrm{v}}\sqrt{1+\tan^2(\zeta)}\right], & h_{\mathrm{v}} \leq \left(\frac{h_{\mathrm{r}}}{D}\right)^{\frac{1}{\alpha}} \\ h_{\mathrm{v}}, & \text{otherwise} \end{cases} \quad (8)$$

$$\alpha = \frac{2(m+3)}{\eta}, \quad (9)$$

and

$$\vartheta_k(u, w, Z_k, \chi) = \int_u^w \chi f_{Z_k}(z) dz. \quad (10)$$

Furthermore, B_{r} and B_{v} are the RF and VLC tier bias factors, respectively [50], and $f_{Z_k}(z)$ represents the probability density function (PDF) of the Euclidean distance between the user and the nearest k^{th} tier BS, which is calculated using the null probability of the PPP [42]

$$f_{Z_{\mathrm{r}}}(z) = 2\pi\lambda_{\mathrm{r}} z \mathrm{e}^{-\pi\lambda_{\mathrm{r}}(z^2 - h_{\mathrm{r}}^2)}, \quad h_{\mathrm{r}} < z < \infty, \quad (11)$$

$$f_{Z_{\mathrm{v}}}(z) = 2\pi\lambda_{\mathrm{v}} z \mathrm{e}^{-\pi\lambda_{\mathrm{v}}(z^2 - h_{\mathrm{v}}^2)}, \quad h_{\mathrm{v}} < z < h_{\mathrm{v}}\sqrt{1+\tan^2(\zeta)}. \quad (12)$$

Proof: See Appendix A.

We note that the association probabilities under RSS given in (5) and (6) depend on the (RF and VLC) BSs' heights and hence are different from [40], which did not include RF BSs' heights in the mathematical analysis. Also, it is worth stating that $A_{\mathrm{VLC}}^{(\mathrm{RSS})} = 1 - A_{\mathrm{RF}}^{(\mathrm{RSS})}$. However, we derive $A_{\mathrm{VLC}}^{(\mathrm{RSS})}$ given in (6) as it will help deriving the service distance distribution. Furthermore, it is noted that $A_{\mathrm{RF}}^{(\mathrm{RSS})} = A_{\mathrm{RF}}^{(\mathrm{OPP})}$ and $A_{\mathrm{VLC}}^{(\mathrm{RSS})} = A_{\mathrm{VLC}}^{(\mathrm{OPP})}$ for $h_{\mathrm{r}} \geq D h_{\mathrm{v}}^{\alpha}(1+\tan^2(\zeta))^{\frac{\alpha}{2}}$. Thus

[2]We use the superscript "(OPP)" to identify quantities associated with the opportunistic VLC policy.

$$A_{\mathrm{RF}}^{(\mathrm{RSS})}=\begin{cases}\underbrace{1-P_0}_{\triangleq A_{\mathrm{RF}_1}}+\underbrace{P_0(1-\mathrm{e}^{-\pi\lambda_{\mathrm{r}}(Dh_{\mathrm{v}}^{\alpha}-h_{\mathrm{r}})(Dh_{\mathrm{v}}^{\alpha}+h_{\mathrm{r}})})}_{\triangleq A_{\mathrm{RF}_2}}+ & h_{\mathrm{r}}\le Dh_{\mathrm{v}}^{\alpha}\\ \underbrace{\vartheta_{\mathrm{r}}\left(Dh_{\mathrm{v}}^{\alpha},\frac{Dh_{\mathrm{v}}^{\alpha}}{(1+\tan^2(\zeta))^{-\frac{\alpha}{2}}},Z_{\mathrm{r}},P_0-1+\mathrm{e}^{-\pi\lambda_{\mathrm{v}}\left(\left(\frac{x}{D}\right)^{\frac{2}{a}}-h_{\mathrm{v}}^2\right)}\right)}_{\triangleq A_{\mathrm{RF}_3}}, & \\ 1-P_0, & h_{\mathrm{r}}\ge\frac{Dh_{\mathrm{v}}^{\alpha}}{(1+\tan^2(\zeta))^{-\frac{\alpha}{2}}}\\ 1-P_0+\vartheta_{\mathrm{r}}\left(h_{\mathrm{r}},\frac{Dh_{\mathrm{v}}^{\alpha}}{(1+\tan^2(\zeta))^{-\frac{\alpha}{2}}},Z_{\mathrm{r}},P_0-1+\mathrm{e}^{-\pi\lambda_{\mathrm{v}}\left(\left(\frac{x}{D}\right)^{\frac{2}{a}}-h_{\mathrm{v}}^2\right)}\right), & \text{Otherwise}\end{cases} \tag{5}$$

$$A_{\mathrm{VLC}}^{(\mathrm{RSS})}=\underbrace{1-\mathrm{e}^{-\pi\lambda_{\mathrm{v}}(Q-h_{\mathrm{v}})(Q+h_{\mathrm{v}})}}_{\triangleq A_{\mathrm{VLC}_1}}+\underbrace{\vartheta_{\mathrm{v}}\left(Q,h_{\mathrm{v}}\sqrt{1+\tan^2(\zeta)},Z_{\mathrm{v}},\mathrm{e}^{-\pi\lambda_{\mathrm{r}}\left(D^2x^{2\alpha}-h_{\mathrm{r}}^2\right)}\right)}_{\triangleq A_{\mathrm{VLC}_2}}, \tag{6}$$

designing an optimal value for D can help balancing the traffic load between the two network tiers under RSS and opportunistic VLC association policies. The probabilities in (5) and (6) can be represented in terms of the Gaussian error function by considering $\alpha=2$, which is omitted for brevity.

B. Service Distance Distributions

Next, we will derive the distributions of the distance between the user and the serving RBS and OBS. The distance distributions are required to obtain the spatial averages realized via averaging out the performance metrics over all user locations. In the opportunistic VLC, the user associates with an OBS wherever it finds VLC coverage. This implies that the cross-tier coverage boundaries in the opportunistic VLC policy do not depend on the locations of the nearby RBSs but depend on the location of OBSs and the receiver FOV instead. Let X_k, $k\in\{\mathrm{r},\mathrm{v}\}$ be the horizontal distances between the user and the projection of the serving BS on the ground provided that the association is with the k^{th} tier BS. Then the PDF of the horizontal distance between the user and the serving RBS can be obtained using the null probability of the PPP and the fact that the user associates to the RBS when $\psi>\zeta$, and it is given by

$$f_{X_{\mathrm{r}}}^{(\mathrm{OPP})}(x)=2\pi\lambda_{\mathrm{r}}\mathrm{e}^{-\pi\lambda_{\mathrm{r}}x^2},\quad 0<x<\infty. \tag{13}$$

Similarly, the PDF of the horizontal distance between the user and the serving OBS can be obtained using the null probability of the PPP as

$$f_{X_{\mathrm{v}}}^{(\mathrm{OPP})}(x)=\frac{2}{P_0}\pi\lambda_{\mathrm{v}}\mathrm{e}^{-\pi\lambda_{\mathrm{v}}x^2},\quad 0<x<h_{\mathrm{v}}\tan(\zeta), \tag{14}$$

where P_0 is defined in (3). Note that the PDF of the distance between the user and the serving RBS i.e., $f_{X_{\mathrm{r}}}^{(\mathrm{OPP})}(x)$, is only required for the characterization of RF-to-RF HO rates. This is because the inter-tier HO boundaries under the opportunistic VLC policy depend only on the locations of the OBSs.

For the RSS policy, we derive the distributions of the distance between the nearby RBS and OBS conditioned on the serving tier, because the cross-tier HO boundaries depend on the locations of RBSs and OBSs. The PDFs of the distances between the user and the serving RBSs and OBSs are given by the following lemma.

Lemma 3 (Distance distributions under RSS policy): The service distance distributions under the RSS association policy can be expressed as

$$f_{X_{\mathrm{r}}}^{(\mathrm{RSS})}(x)=\begin{cases}\dfrac{2\pi\lambda_{\mathrm{r}}x\mathrm{e}^{-\pi\lambda_{\mathrm{r}}x^2}}{A_{\mathrm{RF}_1}(1-\mathrm{e}^{-\pi\lambda_{\mathrm{r}}L_1^2})+A_{\mathrm{RF}_2}}, & 0\le x\le L_{\mathrm{r}_1}\\ \dfrac{2\pi\lambda_{\mathrm{r}}x\mathrm{e}^{-\pi\lambda_{\mathrm{r}}x^2-\pi\lambda_{\mathrm{v}}\left((x^2+h_{\mathrm{r}}^2)^{1/\alpha}D^{-2/\alpha}-h_{\mathrm{v}}^2\right)}}{A_{\mathrm{RF}_1}(\mathrm{e}^{-\pi\lambda_{\mathrm{r}}L_{\mathrm{r}_1}^2}-\mathrm{e}^{-\pi\lambda_{\mathrm{r}}L_{\mathrm{r}_2}^2})+A_{\mathrm{RF}_3}}, & L_{\mathrm{r}_1}<x\le L_{\mathrm{r}_2}\\ \dfrac{(1-P_0)2\pi\lambda_{\mathrm{r}}x\mathrm{e}^{-\pi\lambda_{\mathrm{r}}x^2}}{A_{\mathrm{RF}_1}\mathrm{e}^{-\pi\lambda_{\mathrm{r}}L_{\mathrm{r}_2}^2}}, & L_{\mathrm{r}_2}<x\le\infty\end{cases} \tag{15}$$

$$f_{X_{\mathrm{v}}}^{(\mathrm{RSS})}(x)=\begin{cases}\dfrac{2\pi}{A_{\mathrm{VLC}_1}}\lambda_{\mathrm{v}}x\mathrm{e}^{-\pi\lambda_{\mathrm{v}}x^2}, & 0\le x\le L_{\mathrm{v}}\\ \dfrac{2\pi}{A_{\mathrm{VLC}_2}}\lambda_{\mathrm{v}}x\mathrm{e}^{-\pi\lambda_{\mathrm{v}}x^2}\mathrm{e}^{-\pi\lambda_{\mathrm{r}}(D^2(x^2+h_{\mathrm{v}}^2)^{\alpha}-h_{\mathrm{r}}^2)}, & L_{\mathrm{v}}\le x\le h_{\mathrm{v}}\tan(\zeta)\end{cases} \tag{16}$$

where $A_{\mathrm{RF}_{(.)}}$ and $A_{\mathrm{VLC}_{(.)}}$ have been defined in (5) and (6), respectively, and

$$L_{\mathrm{r}_1}=\begin{cases}\sqrt{D^2h_{\mathrm{v}}^{2\alpha}-h_{\mathrm{r}}^2}, & h_{\mathrm{r}}\le Dh_{\mathrm{v}}^{\alpha}\\ 0, & \text{otherwise}\end{cases},$$

$$L_{\mathrm{r}_2}=\begin{cases}\sqrt{D^2h_{\mathrm{v}}^{2\alpha}(1+\tan^2(\zeta))^{\alpha}-h_{\mathrm{r}}^2}, & h_{\mathrm{r}}\le\frac{Dh_{\mathrm{v}}^{\alpha}}{(1+\tan^2(\zeta))^{-\frac{\alpha}{2}}}\\ 0, & \text{otherwise}\end{cases},$$

$$L_{\mathrm{v}}=\sqrt{Q^2-h_{\mathrm{v}}^2}.$$

Proof: See Appendix B.

We note that the distance distributions under the RSS policy given in (15) and (16) are the conditional distributions conditioned on the serving tier. It is also noted that the conditional distance distributions depend on the BSs' heights.

Since we have obtained the tier association probabilities and the service distance distributions, we will now move on to the characterization of HO boundaries that will eventually lead us to determination of HO rates.

IV. Handover Rates

The overall HO rate is given by

$$H_{\text{Total}} = \sum_{k} \sum_{j} H_{kj}, \tag{17}$$

where H_{kj}, $k, j \in \{\text{r}, \text{v}\}$ is the HO rate between tier-k and tier-j.

A. Handover Rates Characterization Techniques

For the characterization of the individual HO rates, we adopt two different approaches depending upon how the HO boundaries are formed under the two user-to-BS association rules. While the intra-tier HO boundaries under the two rules follow the nearest BS policy, the inter-tier HO boundaries are very different. The inter-tier HO boundaries under RSS consist of a set of points where the biased received powers from the neighboring OBS and RBS are equal. However, under opportunistic VLC policy, the inter-tier HO boundaries depend only on the VLC channel model and the specifications of the receiver photo-detector e.g., FOV. Under this policy, the user performs an RF-to-VLC HO as soon as the target OBS falls within the FOV of the receiver photo-detector. In what follows, we summarize the methods that we used to characterize the HO rates under the two association policies.

1) The *inter-tier HO rates under the opportunistic VLC policy* are characterized by exploiting a very small step movement made by the user and then calculating the probability of crossing the VLC coverage boundary. A similar method was used in [31] to characterize HO probabilities in multi-tier RF networks. 2) The *inter-tier HO rates under RSS policy* are determined by calculating the probability of having the test user on the cell boundaries extended by an infinitesimal width [29]. Due to the distance dependent path-loss model, the inter-tier cell boundaries in the RSS case depend on the locations of the k^{th} and j^{th} tier BSs. Thus, by conditioning on the location of the j^{th} tier BS, we calculate the probability of a test user lying on the kj cell boundary while maintaining the association with k^{th} tier BS. 3) The *intra-tier HO rates under RSS policy* are characterized by considering $k = j$, which also implies the nearest BS association. Under the considered channel gain and path loss models, the intra-tier HO boundaries do not depend on the association policy. Instead, they depend on the distance between the user and the target BS and the respective association probability. Thus, the intra-tier HO rates under RSS can be used to obtain the intra-tier HO rates for the opportunistic VLC policy. Therefore, a separate intra-tier HO analysis for the opportunistic VLC case is not required.

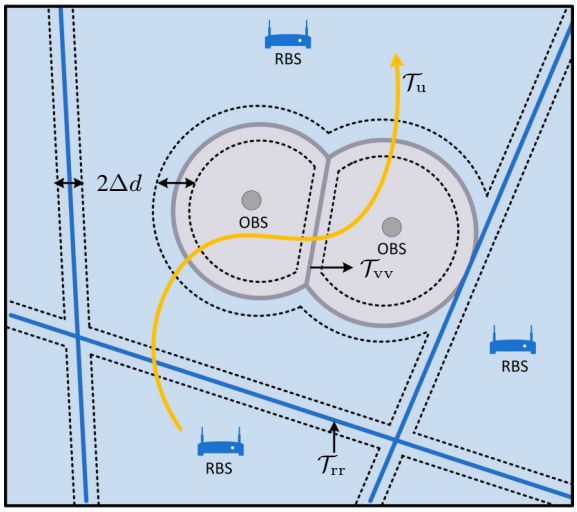

Fig. 3: Two tier Voronoi tessellation showing inter/intra tier HO boundaries between RBS (blue) and OBS (gray). Blue and gray solid lines represent RBS and OBS coverage boundaries, respectively, while black dotted lines represent Δd extended boundaries. $\mathcal{T}_{kj}, k, j \in \{\text{r}, \text{v}\}$ represents the HO boundaries between k and j tier BSs while $\mathcal{T}_{\text{u}}$ represents the user trajectory.

B. Handover Rates with Opportunistic VLC Policy

We start with the derivation of the inter-tier HO rates under the opportunistic VLC policy. This policy implies that the user will perform a handover from RBS to OBS as soon as it enters the coverage area of OBS regardless of the received power. As stated earlier, the coverage area of the OBS depends on the receiver FOV. The user will be in the VLC coverage if $\psi < \zeta$. Therefore, the coverage area of an OBS can be visualized by a circle with radius $h_{\text{v}} \tan(\zeta)$ centered at the projection of the OBS on the ground. Given the current user association with VLC, an inter-tier HO will occur when the distance between the user and the OBS exceeds $h_{\text{v}} \tan(\zeta)$. The inter-tier HO rate under opportunistic VLC user-to-BS association policy is given by the following theorem.

***Theorem** 1:* The inter-tier HO rate in an RF/VLC hybrid network under the opportunistic VLC policy is given by

$$H_{kj}^{(\text{OPP})} = 2\pi\lambda_{\text{v}} P_0 \frac{v}{\ell} \int_0^{h_{\text{v}} \tan(\zeta)} R_{\text{v}} \text{e}^{-\pi\lambda_{\text{v}} R_{\text{v}}^2} \times \cos^{-1}\left(\frac{h_{\text{v}}^2 \tan^2(\zeta) - R_{\text{v}}^2 - \ell^2}{2R_{\text{v}}\ell}\right) dR_{\text{v}}, \quad k \neq j, \tag{18}$$

where ℓ denotes the length of a step taken by the user in a unit time period.

Proof: See Appendix C.

We observe from (18) that the inter-tier HO rate under opportunistic VLC policy does not depend on the RF BSs' parameters (e.g., intensity and height). This is because the opportunistic VLC policy allows users to connect to the OBS as soon as they enter the VLC coverage area.

C. Handover Rates With RSS Policy

Let $H_{kj}^{(\mathrm{RSS})}$ be the tier-k to tier-j HO rate experienced by the test user along its random trajectory $\mathcal{T}_{\mathrm{u}}$ under the RSS association policy. Fig. 3 illustrates a user trajectory through coverage areas and crossing HO boundaries. The HO boundaries between the neighboring BSs are represented by $\mathcal{T}_{kj}$, which corresponds to the set of points where the biased received powers from the nearby RBS and OBS are the same. H_{kj} depends on the number of kj boundary crossings along a trajectory of a certain length and the user velocity. Thus we need to quantify the number of intersections between $\mathcal{T}_{\mathrm{u}}$ and $\mathcal{T}_{kj}$. It is worth mentioning that the mean number of intersections between $\mathcal{T}_{kj}$ and $\mathcal{T}_{\mathrm{u}}$ is equal to the mean number of intersections between $\mathcal{T}_{jk}$ and $\mathcal{T}_{\mathrm{u}}$, which implies that $H_{kj} = H_{jk}$.

In order to quantify the number of intersections between $\mathcal{T}_{kj}$ and $\mathcal{T}_{\mathrm{u}}$ per unit time (i.e., $H_{kj}^{(\mathrm{RSS})}$), we need to first calculate the length intensity $\mu(\mathcal{T}_{kj})$ of cell boundaries, which is defined as the expected length of kj cell boundaries in a unit square. Higher length intensity of cell boundaries gives greater opportunities to the mobile user for boundary crossing, which will increase the overall HO rate. Given $\mu(\mathcal{T}_{kj})$, the HO rate can be expressed as [42]

$$H_{kj}^{(\mathrm{RSS})} = \begin{cases} \frac{2}{\pi}\mu(\mathcal{T}_{kj})v, & \text{for } k = j \\ \frac{1}{\pi}\mu(\mathcal{T}_{kj})v, & \text{for } k \neq j \end{cases}, \tag{19}$$

where $\frac{\cdot}{\pi}\mu(\mathcal{T}_{kj})$ denotes the number of HOs per unit length. The length intensity of cell boundaries can be obtained by calculating the probability of having the test user on the cell boundary. While it is difficult to directly compute this probability, we follow [29] and compute the area intensity $\mu(\mathcal{T}_{kj}^{\Delta d})$ first, which is defined as the expected area of Δd-extended cell boundaries in a unit square. Once we obtain the area intensity, the length intensity of the cell boundaries can be calculated as

$$\mu(\mathcal{T}_{kj}) = \lim_{\Delta d \to 0} \frac{\mu(\mathcal{T}_{kj}^{(\Delta d)})}{2\Delta d}. \tag{20}$$

1) Area Intensity: In this section, we will calculate the area intensity of the cell boundaries. Without loss of generality, we consider a test user located at the origin $\mathbf{0} = (0, 0, 0)$. For the area intensity of the intra-tier cell boundaries (i.e., $k = j$), let $(R_k, 0, h_{\mathrm{k}})$ and $(x_0, y_0, h_{\mathrm{k}})$ represent the locations of the serving and nearby k^{th} tier BSs, respectively. Then $\mathcal{T}_{kj}^{(\mathrm{RSS})}$ is the set of coordinates given by

$$\mathcal{T}_{kj}^{(\mathrm{RSS})} = \Bigg\{ (x,y) \Bigg| (x-x_0)^2 + (y-y_0)^2 = (x-R_{\mathrm{k}})^2 + y^2 \Bigg\}, \quad k = j. \tag{21}$$

For the area intensity of the inter-tier cell boundaries, let the test user be connected to the k^{th} tier BS located at $(R_k, 0, h_k)$, and let (x_0, y_0, h_j) be the location of the closest j^{th} tier BS. Then $\mathcal{T}_{kj}^{(\mathrm{RSS})}$ represents the set of coordinates given by

$$\mathcal{T}_{kj}^{(\mathrm{RSS})} = \Bigg\{ (x,y) \Bigg| (x-x_0)^2 + (y-y_0)^2 + h_j^2 = D^2[(x-R_k)^2 + y^2 + h_k^2]^{\alpha} \Bigg\}, \quad k \neq j, \tag{22}$$

where we used D and α from (7) and (9), respectively. Now the Δd-extended boundaries can be expressed as

$$\mathcal{T}_{kj}^{(\Delta d)} = \left\{ \boldsymbol{u} | \exists \boldsymbol{v} \in \mathcal{T}_{kj}^{(\mathrm{RSS})}, \text{ s.t. } |\boldsymbol{u} - \boldsymbol{v}| < \Delta d \right\}. \tag{23}$$

We note that the area intensity of the cell boundaries is the probability of having the test user located on the extended cell boundary, i.e., $\mathbb{P}[\mathbf{0} \in \mathcal{T}_{kj}^{(\Delta d)}]$. Since the test user could either be associated with the k^{th} or the j^{th} tier BS, we need to condition on the associated tier before reaching to the unconditional area intensity. The area intensity of the intra-tier cell boundaries is given by the following lemma.

Lemma 4: Let R be the horizontal distance between the test user and the serving BS and $\mathbb{P}[\mathbf{0} \in \mathcal{T}_{kk}^{(\Delta d)} | R = R_k, \text{tier} = k]$ be the area intensity of the intra-tier cell boundary, where the association is with the k^{th} tier. Then the conditional area intensity of the cell boundary is given by

$$\mathbb{P}[\mathbf{0} \in \mathcal{T}_{kk}^{(\Delta d)} | R = R_k, n = k] = 2\lambda_k \Delta d \beta(R_k, \theta), \tag{24}$$

where $n \in \{\mathrm{r}, \mathrm{v}\}$ denotes the associated tier and

$$\beta(R_k, \theta) = R_k \int_0^{\pi} \sqrt{2 - 2\cos\theta} d\theta = 4R_k. \tag{25}$$

Proof: See Appendix D.

For the mathematical tractability of area intensity in case of $k \neq j$, we apply the Taylor series expression $f(z) = z^{\alpha} = \alpha z_0^{\alpha-1} z + (1-\alpha) z_0^{\alpha} + \mathcal{O}\left((z - z_0)^2\right)$ with $z \to z_0 = R_k^2 + h_k^2$ to approximate $\mathcal{T}_{kj}^{(\mathrm{RSS})}$ in (22) by

$$\tilde{\mathcal{T}}_{kj}^{(\mathrm{RSS})} = \Bigg\{ (x,y) \Bigg| \frac{1}{D^2}\left[(x-x_0)^2 + (y-y_0)^2 + h_j^2\right] = \alpha(R_k^2 + h_k^2)^{\alpha-1}\left[(x-R_k)^2 + y^2 + h_k^2\right] + (1-\alpha)(R_k^2 + h_k^2)^{\alpha} \Bigg\} \tag{26}$$

using the first degree polynomial only, which offers the following result.

Lemma 5: Let R be the horizontal distance between the test user and the serving BS and $\mathbb{P}[\mathbf{0} \in \tilde{\mathcal{T}}_{kj}^{(\Delta d)} | R = R_k, \text{tier} = k]$ be the area intensity of an approximated kj cell boundary $\tilde{\mathcal{T}}_{kj}^{(\Delta d)}$, where the association is with the k^{th} tier. Then the conditional area intensities of the approximated cell boundaries are given by

$$\mathbb{P}[\mathbf{0} \in \tilde{\mathcal{T}}_{\mathrm{vr}}^{(\Delta d)} | R = R_{\mathrm{v}}, n = \mathrm{v}] = 2\lambda_{\mathrm{r}} \Delta d \beta(R_{\mathrm{v}}, \alpha, D, \theta) + \mathcal{O}(\Delta d^2), \tag{27}$$

$$\mathbb{P}[\mathbf{0} \in \tilde{\mathcal{T}}_{\mathrm{rv}}^{(\Delta d)} | R = R_{\mathrm{r}}, n = \mathrm{r}] = 2\lambda_{\mathrm{v}} \Delta d \beta(R_{\mathrm{r}}, 1/\alpha, D^{-1/\alpha}, \theta) + \mathcal{O}(\Delta d^2), \tag{28}$$

where $\mathcal{O}(.)$ represents the Big-O notation for Δd close to zero and $\beta(R_k, \alpha, D, \theta)$ is given in (29).

$$\beta(R_k,\alpha,D,\theta)=D^2\int_0^{\pi}\sqrt{\frac{D^2(R_k^2+h_{\rm v}^2)^{\alpha}-h_{\rm r}^2}{D^4}-\frac{\alpha R_k}{(R_k^2+h_{\rm v}^2)^{1-\alpha}}\left[\frac{\alpha R_k}{(R_k^2+h_{\rm v}^2)^{1-\alpha}}-\frac{2}{D^2}\sqrt{D^2(R_k^2+h_{\rm v}^2)^{\alpha}-h_{\rm r}^2}\cos(\theta)\right]}d\theta \quad (29)$$

$$\mu(\mathcal{T}_{kj}^{(\Delta d)})=\int\limits_{R_{\rm r}\in S_{\rm r}}2\lambda_{\rm v}\Delta d\beta(R_{\rm r},1/\alpha,D^{-1/\alpha},\theta)f_{X_{\rm r}}^{(\rm RSS)}(R_{\rm r}|n={\rm r})A_{\rm RF}^{(\rm RSS)}dR_{\rm r}+\int\limits_{R_{\rm v}\in S_{\rm v}}2\lambda_{\rm r}\Delta d\beta(R_{\rm v},\alpha,D,\theta)f_{X_{\rm v}}^{(\rm RSS)}(R_{\rm v}|n={\rm v})A_{\rm VLC}^{(\rm RSS)}dR_{\rm v}+\mathcal{O}(\Delta d^2),\quad k\neq j, \quad (30)$$

Proof: See Appendix E.

The Taylor series approximation (26) for $\mathcal{T}_{kj}^{(\rm RSS)}$ has also been used in [52]. The approximation is exact for $\alpha=1$, which results in $\mathcal{T}_{kj}^{(\rm RSS)}$ representing a circle. It is noted from (9) that the range of α depends on the values of m and η, where $0.019\leq m\leq 4.82$ and $2\leq\eta\leq 6$, so that $1<\alpha\leq 7.88$. For this range of α, approximating $\mathcal{T}_{kj}^{(\rm RSS)}$ by a circle as per $\tilde{\mathcal{T}}_{kj}^{(\rm RSS)}$ incurrs a maximum appoximation error of 4%. Hence, the possible approximation error is small and, for the sake of clarity, we present the following results assuming (27) and (28) apply to $\mathcal{T}_{kj}^{(\Delta d)}$.

Since we have obtained the conditional area intensities of the cell boundaries, we can now invoke the association probabilities and the service distance distributions given in Lemmas 2 and 3 to compute the unconditional area intensity.

***Theorem** 2:* The area intensities of Δd-extended cell boundaries are given by (30) and

$$\mu(\mathcal{T}_{kk}^{(\Delta d)})=\int\limits_{R_k\in S_k}2\lambda_k\Delta d\beta(R_k,\theta)f_{X_k}^{(\rm RSS)}(R_k|n=k)A_k^{(\rm RSS)}dR_k,\quad k=j, \quad (31)$$

where the integration regions $S_{\rm r}$ and $S_{\rm v}$ correspond to the BSs' heights dependent boundaries given in (15) and (16), respectively. Similar to [36] and [51], it is intractable to obtain a closed form solution in antennas' height-aware models. Therefore, a numerical evaluation[3] needs to be performed, which is however computationally simple involving only one-dimensional integrals with finite limits.

Proof: See Appendix F.

Since we have derived the area intensity, we can now exploit (20) and calculate the length intensity. Substituting the resulting length intensity in (19) will give the required HO rates under RSS. As stated earlier, the intra-tier HO rates under opportunistic policy follow the same procedure as in RSS. In particular, the intra-tier HO rates under opportunistic policy are obtained by replacing $f_{X_k}^{(\rm RSS)}$ and $A_k^{(\rm RSS)}$ in (31) by $f_{X_k}^{(\rm OPP)}$ and $A_k^{(\rm OPP)}$, respectively. Finally, the overall HO rate under each association policy is calculated by invoking (17).

[3]We use the global adaptive quadrature method for the numerical integration [53].

TABLE II: Simulation parameters in RF/VLC hybrid network [40]

Parameter	**Value**
RBS Power $P_{\rm r}$:	10 dBm
OBS Optical Power $P_{\rm opt}$:	40 dBm
RBS Intensity $\lambda_{\rm r}$:	0.0087 BS/m^2
OBS Intensity $\lambda_{\rm v}$:	0.1648 BS/m^2
BSs' heights $h_{\rm r}$, $h_{\rm v}$:	2.5 m, 2.5 m
Refractive Index n:	1.5
Path loss exponent η:	3.5
Photo-detector Area $A_{\rm pd}$:	0.0001 m^2
Photo-detector Responsivity $R_{\rm pd}$:	0.6 A/W
Gain of Optical Filter $T(\zeta)$:	1
Optical-to-electrical conversion ratio $n_{\rm c}$:	3
Half-power Semi-angle $\Phi_{1/2}$:	60^o
Carrier Frequency $f_{\rm c}$:	2.4 GHz
User velocity v:	0.28 m/s

2) A Special Case $\left(P^{\rm VLC}>P^{\rm RF},\ \psi=\zeta\right)$: Depending upon the power disparity between the RBSs and OBSs, there could be a situation where $\mathcal{T}_{kj}^{(\rm RSS)}$ in (22) is an empty set. This occurs when $P^{\rm VLC}>P^{\rm RF}$ and $\psi=\zeta$. Thus if a user located on the cross-tier boundary moves away from the serving OBS such that $\psi>\zeta$ then $P^{\rm VLC}$ will drop to zero because of the DC channel gain dependency on ψ as shown in (2). In such a case the type kj HO can be captured via the opportunistic VLC policy, which states that the cross-tier HOs are performed when $\psi=\zeta$. Considering the aforementioned situation, the overall inter-tier HO rate under RSS policy will be the weighted sum of the HOs occurring within the coverage area of OBS ($\psi<\zeta$) and the HOs occurring at the boundary ($\psi=\zeta$), which is given as

$$H_{kj}^{(\rm RSS)'}=\left(1-\frac{A_{\rm RF_1}}{A_{\rm RF}^{(\rm RSS)}}\right)H_{kj}^{(\rm RSS)}+\frac{A_{\rm RF_1}}{A_{\rm RF}^{(\rm RSS)}}H_{kj}^{(\rm OPP)}, \quad (32)$$

where $A_{\rm RF_1}$ is defined in (5), $H_{kj}^{(\rm RSS)}$ is given in (19), and $H_{kj}^{(\rm OPP)}$ is the inter-tier HO rate under opportunistic VLC user-to-BS association policy, which is given in (18).

V. Numerical Results

We will now exploit the mathematical framework presented in this paper to quantify the impact of user mobility and VLC centric parameters on the user-to-BS association probabilities and the HO rates in RF/VLC hybrid networks. The developed mathematical model does not only help analyzing the

relationship between different network parameters but also offers a basis for future handover management related studies. Here, we analyze the impact of user mobility and receiver FOV on user-to-BS association probabilities and HO rates under the four deployment models in Fig. 1. First, we validate the accuracy of analytical PPP modeling via Monte-Carlo simulations. Then, we simulate the other deployment models (i.e., square lattice, MHCPP, and actual deployment) and analyze the performance metrics with respect to the receiver FOV under all deployment models.

A. Simulation Setup

In order to conduct a fair performance comparison, we adopt the simulation area and the parameters in accordance with the actual scenario in all deployment cases. We consider a simulation area of 74 m x 31 m, which is the area of an academic block in the University of British Columbia, Canada. In the actual deployment case, we import the actual number of RBSs and luminaries along with their x-y coordinates into the simulation tool. We calculate the corresponding BSs intensities and use that for generating the PPP in the PPP deployment case and abstracting the BSs' locations in the square lattice case. For MHCPP, first, we generate a PPP $\acute{\Phi}_k$ with intensity $\acute{\lambda_k}$. Then, each point in the PPP is marked with a random number, which is independently and uniformly distributed on $[0, 1]$. A point is retained in the point process $\acute{\Phi}_k$ if its mark is the largest among all the points within a distance d_k and is removed otherwise. In order to have a fair comparison, the intensity of initial PPP $\acute{\Phi}_k$ is considered higher than that of λ_k, i.e., $\acute{\lambda_k} = -\ln(1 - \lambda_k \pi d_k^2)/\pi d_k^2$ [42].

In all deployment cases, we consider a test mobile user following the random way-point mobility model. The user moves a distance of 0.05 m in each step taken in a random direction with 1300 steps in each iteration, where there are 2000 iterations in total. Within each iteration, the initial location of the user is chosen uniformly at random within the simulation area in the actual and square lattice deployments while independent PPPs with the given intensities are generated in the PPP deployment case. After each step taken by the user, the current and the new associations are recorded, which are then used to calculate the tier association probability and intra/inter-tier HO rates. The performance metrics are then averaged over the total number of iterations. We consider unity bias factors unless stated otherwise. The simulation parameters are summarized in Table II where the RF parameters are the actual parameters of an indoor Wi-Fi network deployed in the university academic block and the VLC specific parameters are in accordance with [40].

B. Association Analysis

First, we consider the association probabilities and the impact of the receiver FOV in RF/VLC hybrid networks under different deployment models. Figs. 4(a) and 4(b) show the association comparison among different BSs' locations abstraction models under the RSS and opportunistic VLC policies, respectively. We observe that user-to-OBS association probability reaches up to 40% under RSS policy and then decreases monotonically for a FOV $> 30°$. This is due to the fact that the concentrator gain varies with the photo-detector FOV, i.e., $G(\zeta)$. However, the user-to-OBS association probability shows an increasing trend in case of opportunistic VLC because the coverage footprint of VLC increases with the FOV. It is also worth noting that the PPP simulation results validate the mathematical analysis. While the association trends with the square lattice deployment are a bit far from the actual ones over the FOV range of about $30°$ to $60°$ under the RSS policy, it is observed that the PPP and the MHCPP show a close match with the actual deployment over the complete FOV range. It is also observed that a lower inter-BS distance threshold in MHCPP leads to PPP-like performance. Furthermore, the PPP, the MHCPP, and the square lattice deployments conform with the trends from the actual deployment under opportunistic VLC policy. Hence, our quantitative results suggest the use of PPP based analytical modelling in association related studies in RF/VLC hybrid networks.

C. Handover Rates Analysis

Next, we consider results for HO rates under different deployment models and association policies and highlight the impact of the receiver FOV. Figs. 5(a) and 5(b) show the intra and inter-tier HO rates in PPP based RF/VLC hybrid networks for the two association policies. From Fig. 5(a), we observe that the overall HO rate in the RSS policy decreases when FOV exceeds 20^o. This is because the VLC gets under-utilized with the increase in the FOV, which limits the inter-tier HO rates. On the other hand, opportunistic VLC based HO rates show a constant trend for FOV $> 50^o$ with VLC-to-VLC HOs being the only contributor. The results also indicate that the HO rates have negligible dependency on the FOV for FOV$> 60^o$ regardless of the association policy. Moreover, an overlap between the PPP based analytical results and the simulation results is also observed. The HO rates under different deployment models are shown in Fig. 6(a) for the RSS policy and in Fig. 6(b) for the opportunistic VLC policy. Again, it is observed that the PPP, the MHCPP, and the square lattice models are all good approximations as they capture the performance of an actual network. It is also observed that the MHCPP with the higher d_k leads to even better approximation of the HO rates. Conclusively, the numerical results suggest the following: i) RF/VLC hybrid networks can be modelled via PPP and ii) PPP based mathematical model presented in this paper can be used as a baseline to conduct HO management related studies.

D. Effect of Biasing

It is evident from the Fig. 4(b) that the VLC association probability reaches one, which renders the RF tier under-utilized. This causes an increase in VLC-to-VLC HO rates (see Fig. 5(b)). Similarly, it is noted from the Fig. 4(a) that the VLC tier gets under-utilized for a FOV $> 50^o$, which causes an increase in RF-to-RF HO rates. In order to address this issue, we incorporate the bias factor in the analysis to balance the tradeoff between the network utilization and the HO rates. Figs. 7(a) and 7(b) show the impact of biasing on the PPP

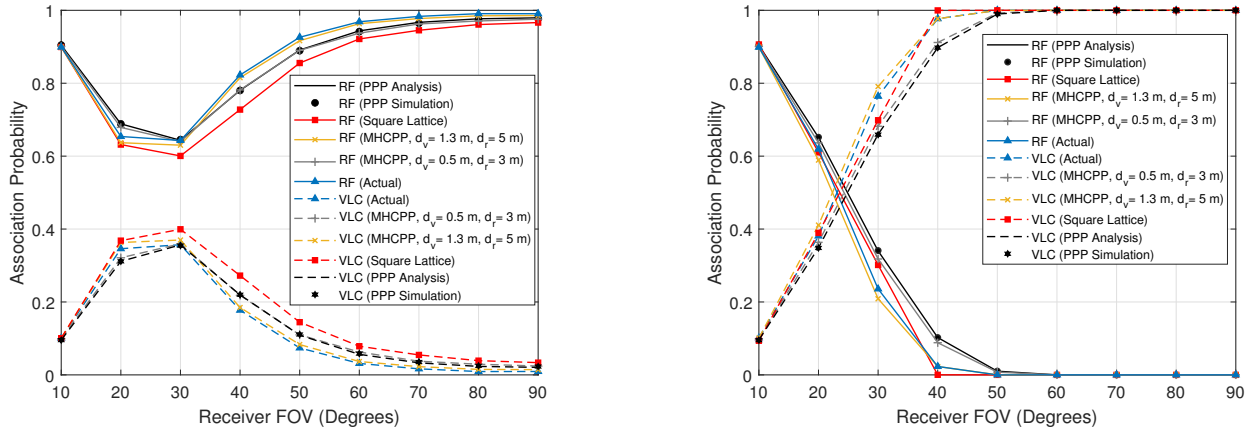

(a) RSS (b) Opportunistic VLC

Fig. 4: Comparison of association probabilities under different BSs' deployment models.

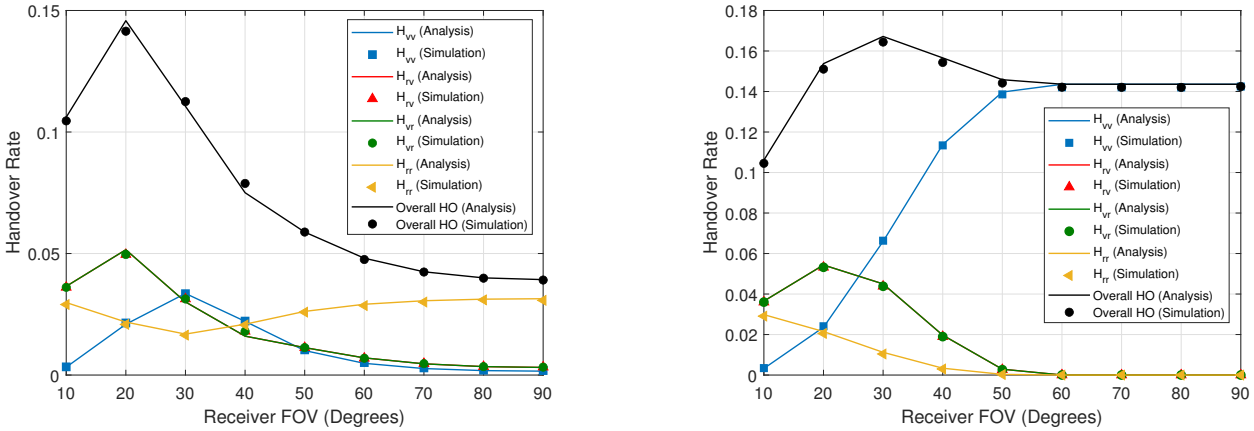

(a) RSS (b) Opportunistic VLC

Fig. 5: HO rates in PPP based RF/VLC hybrid network.

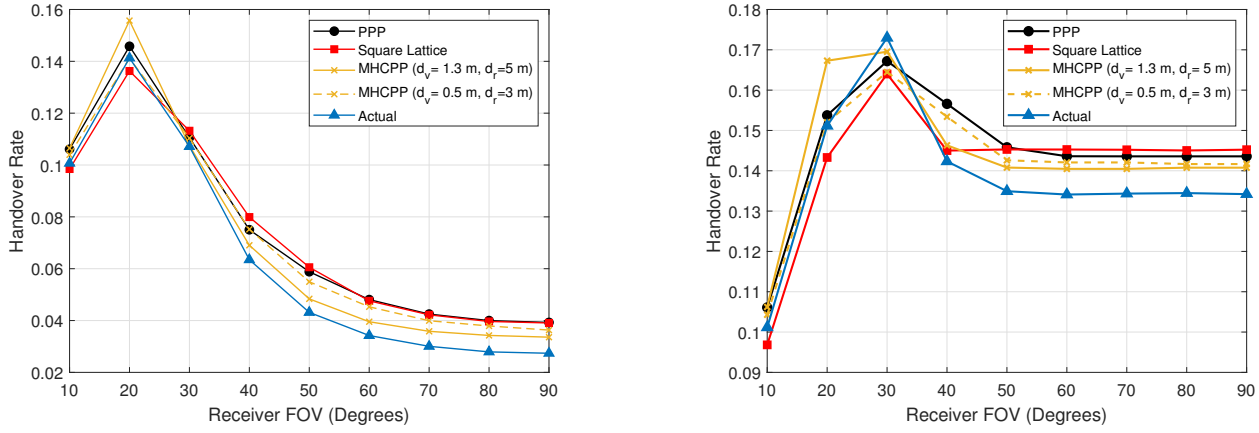

(a) RSS (b) Opportunistic VLC

Fig. 6: Comparison of HO rates under different BSs' deployment models.

based association probabilities and HO rates, respectively. We observe that a 4 dB bias offers a balance in the association probabilities (see red lines in Fig. 7(a)) of RF and VLC tiers. In particular, the RF and VLC association probabilities are 52% and 48%, respectively with FOV $= 50^o$. Moreover, the biasing also reduces the overall HO rate when compared to the ones with the opportunistic VLC policy. While the biased RSS association policy may help balancing the tradeoff between network utilization and HO rates, the performance directly depends on the bias value, which can be computed using the mathematical model presented in this paper.

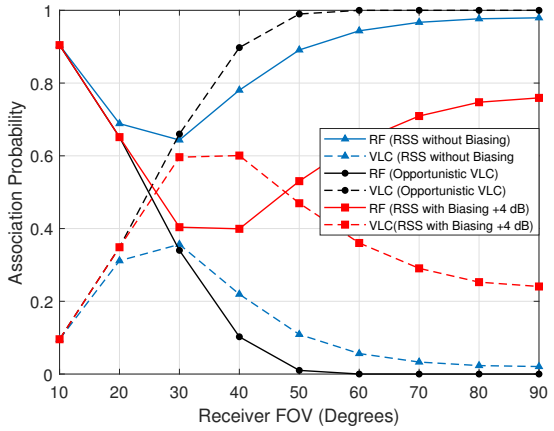

(a) Association probabilities

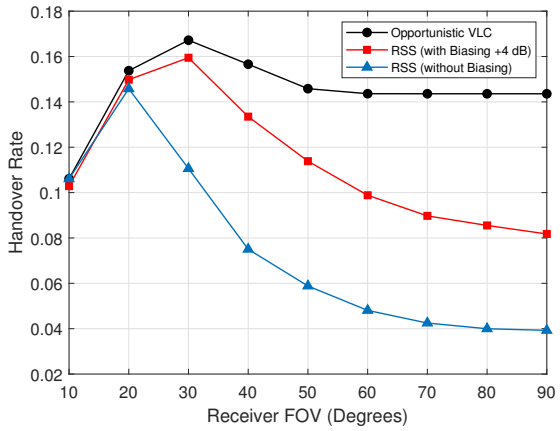

(b) HO Rates

Fig. 7: Impact of biasing on the PPP association probabilities and HO rates with $B_{\mathrm{v}} = 4$ dB.

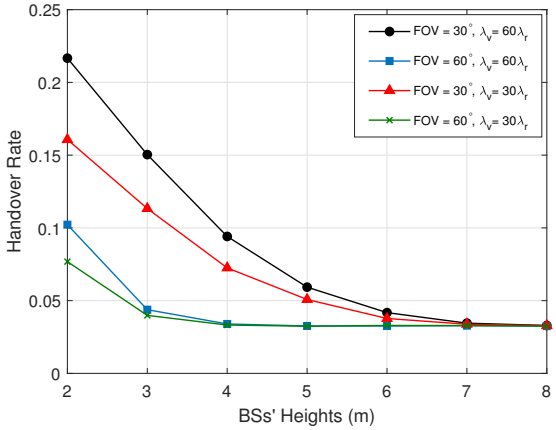

(a) RSS

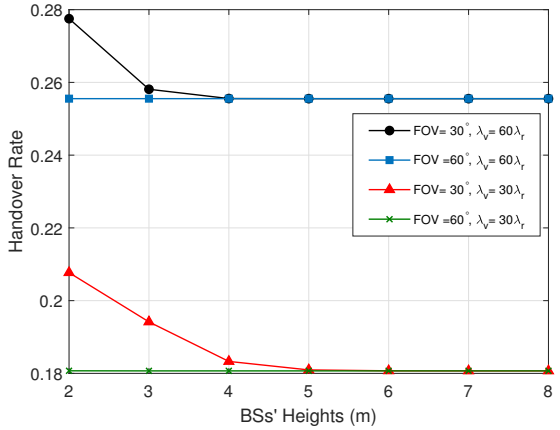

(b) Opportunistic VLC

Fig. 8: Impact of BSs' heights on the PPP handover rates.

E. Effect of BSs' Heights

Next, we study the impact of BSs' heights on the HO rates under different OBSs' intensities and receiver FOVs. Since one of the main objectives behind OBSs deployment is offloading existing RF spectrum, we have kept the RBSs intensity to be constant. Figs. 8(a) and 8(b) show the impact of BSs' heights on the PPP HO rates under RSS and opportunistic VLC association policies, respectively. It is evident from the trends that the HO rates increase{decrease} with the increasing OBS intensity{BSs' height} except for FOV$= 60°$ in opportunistic VLC case where the high OBS intensities dominate the RF coverage area. However, regardless of the association policy, there comes a point where the BSs' height have no impact on the handover rates. Thus, the mathematical model presented in this paper can help determining the appropriate BSs' heights to achieve the desired HO rates against the given BSs' intensity and receiver FOV.

VI. Conclusion

This paper characterized the association probabilities and HO rates in PPP based two-tier RF/VLC hybrid networks. Two different user-to-BS association policies namely RSS and opportunistic VLC were considered, and the PPP based analytical results were compared with the simulated results for an MHCPP, a square lattice, and an actual deployment. The results indicate that all the PPP, the MHCPP, and the square lattice deployments are good approximations for abstracting the BSs' locations in RF/VLC hybrid networks. This advocates the usefulness and applicability of PPP based mathematical modeling in RF/VLC hybrid network. The results also indicate that the two association policies allow one tier to capture more traffic at the expense of increased HO rates. Therefore, biasing is proposed to balance the tradeoff between the association probabilities and the HO rates. Along with the quantification of the impact of network parameters on the HO rates, the mathematical framework developed in this paper offers a basis to conduct further HO management studies (e.g., towards reducing HOs) and quantifying the effect of HO rate on the user throughput in RF/VLC hybrid networks.

Appendix

A. Proof of Lemma 2

The RF association probability in the RSS case can be written as

$$A_{\mathrm{RF}}^{(\mathrm{RSS})} = \mathbb{P}[P^{\mathrm{RF}} > P^{\mathrm{VLC}}] = \mathbb{P}[P^{\mathrm{RF}} > P^{\mathrm{VLC}}, \psi > \zeta] + \mathbb{P}[P^{\mathrm{RF}} > P^{\mathrm{VLC}}, \psi < \zeta]. \quad (33)$$

Since $G = 0$ when $\psi > \zeta$, which implies that $P^{\mathrm{VLC}} = 0$, the first term of (33) is

$$\mathbb{P}[P^{\mathrm{RF}} > P^{\mathrm{VLC}}, \psi > \zeta] = \mathbb{P}[\psi > \zeta] = 1 - P_0, \quad (34)$$

where P_0 is defined in Lemma 1. Furthermore, letting Z_k be the Euclidean distance between the user and the nearest k-tier BS, the second term in (33) can be written as

$$\mathbb{P}[P^{\mathrm{RF}} > P^{\mathrm{VLC}}, \psi < \zeta] = \mathbb{E}_{Z_{\mathrm{r}}}\left\{\mathbb{P}\big[Z_{\mathrm{v}} > \big(\frac{Z_{\mathrm{r}}}{D}\big)^{\frac{1}{\alpha}}, Z_{\mathrm{v}} < h_{\mathrm{v}}\sqrt{1+\tan^2(\zeta)}\big]\right\}. \quad (35)$$

The joint probability $\mathbb{P}\big[.,.\big]$ on the right hand side in (35) becomes $\mathbb{P}\big[Z_{\mathrm{v}} < h_{\mathrm{v}}\sqrt{1+\tan^2(\zeta)}\big] \triangleq P_0$ for $h_{\mathrm{r}} < Z_{\mathrm{r}} \leq Dh_{\mathrm{v}}^{\alpha}$ and $F_{Z_{\mathrm{v}}}(h_{\mathrm{v}}\sqrt{1+\tan^2(\zeta)}) - F_{Z_{\mathrm{v}}}((\frac{Z_{\mathrm{r}}}{D})^{\frac{1}{\alpha}})$ for $Dh_{\mathrm{v}}^{\alpha} < Z_{\mathrm{r}} \leq \frac{Dh_{\mathrm{v}}^{\alpha}}{(1+\tan^2(\zeta))^{-\frac{\alpha}{2}}}$, where $F_{Z_{\mathrm{v}}}(z) = 1 - \mathrm{e}^{-\pi\lambda_{\mathrm{v}}(z^2 - h_{\mathrm{v}}^2)}$ represents the cumulative distribution function (CDF) of the distance between the user and the OBS obtained using the PDF in (12). Then taking the expectation over Z_{r} using the PDF given in (11) will yield the RF association probability shown in (5).

The VLC association probability in the RSS case can be written as

$$A_{\mathrm{VLC}}^{(\mathrm{RSS})} = \mathbb{P}[P^{\mathrm{VLC}} > P^{\mathrm{RF}}] = \mathbb{P}[P^{\mathrm{VLC}} > P^{\mathrm{RF}}, \psi < \zeta] + \mathbb{P}[P^{\mathrm{VLC}} > P^{\mathrm{RF}}, \psi > \zeta]. \quad (36)$$

Since $G = 0$ for $\psi > \zeta$, the VLC association probability becomes $A_{\mathrm{VLC}}^{(\mathrm{RSS})} = \mathbb{P}[P^{\mathrm{VLC}} > P^{\mathrm{RF}}, \psi < \zeta]$. Further mathematical manipulation leads to

$$A_{\mathrm{VLC}}^{(\mathrm{RSS})} = \mathbb{E}_{Z_{\mathrm{r}}}\left\{\mathbb{P}[Z_{\mathrm{r}} > DZ_{\mathrm{v}}^{\alpha}, \psi < \zeta]\right\} \quad (37)$$

and

$$\mathbb{P}[Z_{\mathrm{r}} > DZ_{\mathrm{v}}^{\alpha}, \psi < \zeta] = \begin{cases} 1, & h_{\mathrm{v}} < Z_{\mathrm{v}} < Q \\ \mathrm{e}^{-\pi\lambda_{\mathrm{r}}\left(D^2 Z_{\mathrm{v}}^{2\alpha} - h_{\mathrm{r}}^2\right)}, & \left(\frac{h_{\mathrm{r}}}{D}\right)^{1/\alpha} < Z_{\mathrm{v}} < h_{\mathrm{v}}\sqrt{1+\tan^2(\zeta)} \end{cases}. \quad (38)$$

Then taking the expectation over Z_{v} in (37) with the PDF given in (12) gives the association probability shown in (6).

B. Proof of Lemma 3

Let X_k be the horizontal distance between the user and the serving k^{th} tier BS. Then the conditional PDF of the distance between the user and the serving BS can be calculated by determining the complementary cumulative distribution function (CCDF) given that the user associates with the k^{th} tier. Hence,

$$\mathbb{P}[X_k > x] = \mathbb{P}[R_k > x \big| n = k] = \frac{\mathbb{P}[R_k > x, n = k]}{\mathbb{P}[n = k]}, \quad (39)$$

where $\mathbb{P}[n = k] = A_k$ represents the k^{th} tier association probability, which is given in Lemma 2. Next, we exploit the null probability of the PPP to calculate the joint distribution $\mathbb{P}[R_k > x, n = k]$. Then, we invoke the tier association probabilities conditioned on the heights in (5) and (6). Finally, we take the derivative with respect to x to obtain the service distance distributions given in (15) and (16).

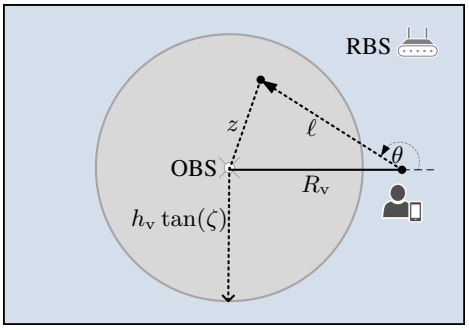

Fig. 9: Handover modeling under opportunistic VLC policy.

C. Proof of Theorem 1

Let the test user connected with the RBS move a small distance of length ℓ forming an angle θ with respect to the direction of the connection (see Fig. 9). Then $z^2 = R_{\mathrm{v}}^2 + \ell^2 + 2R_{\mathrm{v}}\ell\cos(\theta)$ is the Euclidean distance between the OBS and the new location of the user. The probability of an inter-tier HO is the probability that the user enters the VLC coverage area and thus

$$\mathbb{P}[\text{Inter-tier HO}] = \mathbb{P}[z < h_{\mathrm{v}}\tan(\zeta)]. \quad (40)$$

Substituting z in (40) gives

$$\mathbb{P}[\text{Inter-tier HO}] = \mathbb{E}_{R_{\mathrm{v}}}\left\{\mathbb{P}\left[\theta < \cos^{-1}\left(\frac{h_{\mathrm{v}}^2\tan^2(\zeta) - R_{\mathrm{v}}^2 - \ell^2}{2R_{\mathrm{v}}\ell}\right)\right]\right\}, \quad (41)$$

where θ is uniformly distributed over the interval $[0, \pi]$. Invoking the distribution of a uniformly distributed random variable and taking the expectation w.r.t. R_{v} given in (14) and multiplying with $A_{\mathrm{VLC}}^{(\mathrm{OPP})}$ gives the desired inter-tier HO probability. Finally, multiplying the HO probability with v/ℓ with yields the inter-tier HO rate shown in Theorem 1.

D. Proof of Lemma 4

Mathematical manipulation of (21) leads to

$$\mathcal{T}_{kk}^{(\mathrm{RSS})} = \left\{(x, y)\middle|(R_k - x_0)x - y_0 y + \frac{x_0^2 + y_0^2 - R_k^2}{2} = 0\right\}, \quad (42)$$

which represents the equation of a line. Then the distance d from $\mathbf{0}$ to the line is given by

$$d = \frac{\big|x_0^2 + y_0^2 - R_k^2\big|/2}{\sqrt{(R_k - x_0)^2 + y_0^2}}. \quad (43)$$

Let $\mathcal{S}_{kk} = \big\{x_0, y_0 | d < \Delta d\big\}$ be the set of all possible locations of the nearby k-tier BS such that the condition $\mathbf{0} \in \mathcal{T}_{kk}^{(\mathrm{RSS})}$ is satisfied. Using the expression for d in (43), we can write $\mathcal{S}_{kk}$ as

$$\mathcal{S}_{kk} = \left\{x_0, y_0 \middle| \frac{\big|x_0^2 + y_0^2 - R_k^2\big|/2}{\sqrt{(R_k - x_0)^2 + y_0^2}} < \Delta d\right\}. \quad (44)$$

Converting (x_0, y_0) into polar coordinates ($r = \sqrt{x_0^2+y_0^2}, \theta = \tan^{-1}(y_0/x_0)$) and the fact that $r > R_k$, we get

$$|\mathcal{S}_{\rm kk}| = 2\int_0^{\pi}\int_{R_k}^{\sqrt{R_k^2+2\Delta d R_k\sqrt{2-2\cos(\theta)}}} r dr d\theta$$
$$= 2\Delta d R_k \int_0^{\pi}\sqrt{2-2\cos(\theta)}d\theta = 2\Delta d\beta(R_k,\theta). \quad (45)$$

Then the conditional area intensity in (24) is obtained by invoking the null probability of PPP i.e., no $k^{\rm th}$ tier BS exists in $|\mathcal{S}_{kk}|$:

$$\mathbb{P}[\mathbf{0}\in\mathcal{T}_{kk}^{(\Delta d)}|R=R_k,n=k] = 1-{\rm e}^{-\lambda_k|\mathcal{S}_{\rm kk}|}$$
$$= 2\Delta d\lambda_k\beta(R_k,\theta). \quad (46)$$

E. Proof of Lemma 5

Consider the Taylor series based approximation $\tilde{\mathcal{T}}_{kj}^{(\rm RSS)}$ in (26) for $\mathcal{T}_{kj}^{(\rm RSS)}$ in (22). Let the test user is connected to the OBS (i.e., $k = {\rm v}$ and $j = {\rm r}$), then rearranging (26) leads to

$$\tilde{\mathcal{T}}_{\rm vr}^{(\rm RSS)} = \left\{(x,y)\middle|(x-a)^2+(y-b)^2=r^2\right\}, \quad (47)$$

which represents the equation of a circle centered at (a, b) with radius r, where

$$a = \frac{D^{-2}x_0-\alpha R_{\rm v}(R_{\rm v}^2+h_{\rm v}^2)^{\alpha-1}}{D^{-2}-\alpha(R_{\rm v}^2+h_{\rm v}^2)^{\alpha-1}},$$
$$b = \frac{D^{-2}y_0}{D^{-2}-\alpha(R_{\rm v}^2+h_{\rm v}^2)^{\alpha-1}},$$
$$r^2 = \frac{(R_{\rm v}^2+h_{\rm v}^2)^{\alpha}-D^{-2}(x_0^2+y_0^2+h_{\rm r}^2)}{D^{-2}-\alpha(R_{\rm v}^2+h_{\rm v}^2)^{\alpha-1}} + \frac{(D^{-2}x_0-\alpha R_{\rm v}(R_{\rm v}^2+h_{\rm v}^2)^{\alpha-1})^2+D^2y_0^2}{[D^{-2}-\alpha(R_{\rm v}^2+h_{\rm v}^2)^{\alpha-1}]^2}.$$

Now, the distance d from $\mathbf{0} = (0, 0, 0)$ to the trace can be obtained as shown below. Next, let $\mathcal{S}_{kj} = \{x_0, y_0|d < \Delta d\}$ be the set of all possible locations of the closest j-tier BS such that the condition $\mathbf{0} \in \tilde{\mathcal{T}}_{kj}^{(\rm RSS)}$ is satisfied. Then, we use the expression for d in (48) and note that $\frac{\sqrt{a'}-\sqrt{b'}}{c} < \Delta d$ is equivalent to $|a'-b'| < c\Delta d\sqrt{2(a'+b')+\mathcal{O}(\Delta d^2)}$, to arrive at

$$\mathcal{S}_{\rm vr} = \left\{x_0,y_0\middle|x_0^2+y_0^2 < D^2(R_{\rm v}^2+h_{\rm v}^2)^{\alpha}-h_{\rm r}^2+ D^2\Delta d\sqrt{2(a'+b')+\mathcal{O}(\Delta d^2)}\right\}. \quad (49)$$

Converting (x_0, y_0) into polar coordinates and the fact that $r > \sqrt{D^2(R_{\rm v}^2+h_{\rm v}^2)^{\alpha}-h_{\rm r}^2}$, we have

$$|\mathcal{S}_{\rm vr}| = 2\int_0^{\pi}\int_{\sqrt{D^2(R_{\rm v}^2+h_{\rm v}^2)^{\alpha}-h_{\rm r}^2}}^{\sqrt{D^2(R_{\rm v}^2+h_{\rm v}^2)^{\alpha}-h_{\rm r}^2+D^2\Delta d\sqrt{2(a'+b')+\mathcal{O}(\Delta d^2)}}} r dr d\theta$$
$$= 2\Delta d\beta(R_{\rm v},\alpha,D,\theta)+\mathcal{O}(\Delta d^2). \quad (50)$$

Then (27) is obtained by invoking the null probability of the PPP, i.e., no RBS exists in $|\mathcal{S}_{\rm vr}|$:

$$\mathbb{P}[\mathbf{0}\in\tilde{\mathcal{T}}_{\rm vr}^{(\Delta d)}|x=R_{\rm v},n={\rm v}] = 1-{\rm e}^{-\lambda_{\rm r}|\mathcal{S}_{\rm vr}|}$$
$$= 2\Delta d\lambda_{\rm r}D^2\beta(R_{\rm v},\alpha,D,\theta)+\mathcal{O}(\Delta d^2). \quad (51)$$

We follow a similar approach to calculate $\mathbb{P}[\mathbf{0}\in\tilde{\mathcal{T}}_{\rm rv}^{(\Delta d)}|R=R_{\rm r},n={\rm r}]$ in (28). In particular, we consider $k = {\rm r}$ and $j = {\rm v}$ in (26) and follow the steps from (47) to (51) to obtain (28).

F. Proof of Theorem 2

Let $\mu(\mathcal{T}_{kj}^{(\Delta d)})$ be the area intensity of cell boundaries, which is equal to the probability of having an arbitrary point on the extended cell boundary. This implies that

$$\mu(\mathcal{T}_{kj}^{(\Delta d)}) = \mathbb{P}[\mathbf{0}\in\mathcal{T}_{kj}^{(\Delta d)}]$$
$$=\int_{R_{\rm v}\in S_{\rm v}}\mathbb{P}[\mathbf{0}\in\mathcal{T}_{kj}^{(\Delta d)}|X=R_{\rm v},n={\rm v}]f_{X_{\rm v}}(R_{\rm v}|n={\rm v})\mathbb{P}[n={\rm v}]dR_{\rm v}$$
$$+\int_{R_{\rm r}\in S_{\rm r}}\mathbb{P}[\mathbf{0}\in\mathcal{T}_{kj}^{(\Delta d)}|X=R_{\rm r},n={\rm r}]f_{X_{\rm r}}(R_{\rm r}|n={\rm r})\mathbb{P}[n={\rm r}]dR_{\rm r}, \quad (52)$$

where the integration regions $S_{\rm v}$ and $S_{\rm r}$ correspond to the height dependent boundaries given in (15) and (16), respectively. The theorem is proved by the substitution of (5), (6), (15), (16), (27), and (28) in (52).

REFERENCES

[1] N. Bhushan, J. Li, D. Malladi, R. Gilmore, D. Brenner, A. Damnjanovic, R. T. Sukhavasi, C. Patel, and S. Geirhofer, "Network densification: the dominant theme for wireless evolution into 5G," *IEEE Communications Magazine*, vol. 52, no. 2, pp. 82–89, 2014.

[2] A. Anpalagan, M. Bennis, and R. Vannithamby, *Design and deployment of small cell networks*. Cambridge University Press, 2015.

[3] Huawei, "5G-Oriented indoor digitalization solution," *White paper*, 2017, available at http://www-file.huawei.com/-/media/corporate/pdf/mbb/5g_oriented_indoor_digitalization_solution_white_paper_en.pdf.

[4] R. Bian, I. Tavakkolnia, and H. Haas, "15.73 Gb/s visible light communication with off-the-shelf LEDs," *IEEE Journal of Lightwave Technology*, vol. 37, no. 10, pp. 2418–2424, 2019.

[5] H. Elgala, R. Mesleh, and H. Haas, "Indoor optical wireless communication: potential and state-of-the-art," *IEEE Communications Magazine*, vol. 49, no. 9, pp. 56–62, 2011.

[6] D. A. Basnayaka and H. Haas, "Hybrid RF and VLC systems: Improving user data rate performance of VLC systems," in *IEEE 81st Vehicular Technology Conference (VTC Spring)*, 2015, pp. 1–5.

[7] S. Shao, A. Khreishah, M. B. Rahaim, H. Elgala, M. Ayyash, T. D. Little, and J. Wu, "An indoor hybrid WiFi-VLC internet access system," in *IEEE 11th International Conference on Mobile Ad Hoc and Sensor Systems*, 2014, pp. 569–574.

[8] Case studies archive - purelife. Accessed: 2020-03-24. [Online]. Available: https://purelifi.com/case-studies/

[9] M. Kashef, M. Abdallah, and N. Al-Dhahir, "Transmit power optimization for a hybrid PLC/VLC/RF communication system," *IEEE Transactions on Green Communications and Networking*, vol. 2, no. 1, pp. 234–245, 2017.

[10] A. Khreishah, S. Shao, A. Gharaibeh, M. Ayyash, H. Elgala, and N. Ansari, "A hybrid RF-VLC system for energy efficient wireless access," *IEEE Transactions on Green Communications and Networking*, vol. 2, no. 4, pp. 932–944, 2018.

[11] D. A. Basnayaka and H. Haas, "Design and analysis of a hybrid radio frequency and visible light communication system," *IEEE Transactions on Communications*, vol. 65, no. 10, pp. 4334–4347, 2017.

[12] J. Kong, M. Ismail, E. Serpedin, and K. A. Qaraqe, "Energy efficient optimization of base station intensities for hybrid RF/VLC networks," *IEEE Transactions on Wireless Communications*, vol. 18, no. 8, pp. 4171–4183, 2019.

[13] S. Ma, F. Zhang, H. Li, F. Zhou, M.-S. Alouini, and S. Li, "Aggregated VLC-RF systems: Achievable rates, optimal power allocation, and energy efficiency," *IEEE Transactions on Wireless Communications*, vol. Early Access Article, 2020.

$$d = \frac{\sqrt{(\frac{x_0}{D^2} - \alpha R_{\mathrm{v}}(R_{\mathrm{v}}^2+h_{\mathrm{v}}^2)^{\alpha-1})^2 + \frac{y_0^2}{D^4}}}{D^{-2} - \alpha(R_{\mathrm{v}}^2+h_{\mathrm{v}}^2)^{\alpha-1}} - \frac{\sqrt{[\frac{1}{D^2} - \alpha(R_{\mathrm{v}}^2+h_{\mathrm{v}}^2)^{\alpha-1}][(R_{\mathrm{v}}^2+h_{\mathrm{v}}^2)^{\alpha} - \frac{(x_0^2+y_0^2+h_{\mathrm{r}}^2)}{D^2}] + (\frac{x_0}{D^2} - \alpha R_{\mathrm{v}}(R_{\mathrm{v}}^2+h_{\mathrm{v}}^2)^{\alpha-1})^2 + \frac{y_0^2}{D^4}}}{D^{-2} - \alpha(R_{\mathrm{v}}^2+h_{\mathrm{v}}^2)^{\alpha-1}} \triangleq \frac{\sqrt{a'} - \sqrt{b'}}{c}. \quad (48)$$

[14] X. Ge, S. Tu, G. Mao, C.-X. Wang, and T. Han, "5G ultra-dense cellular networks," *IEEE Wireless Communications*, vol. 23, no. 1, pp. 72–79, 2016.

[15] J. Wu, M. Chen, C. Hu, and G. Zhang, "FC-WiFi: An OpenFlow based WiFi network with free configuration," in *IEEE Ninth International Conference on Frontier of Computer Science and Technology*, 2015, pp. 52–58.

[16] M. Tayyab, G. P. Koudouridis, X. Gelabert, and R. Jäntti, "Signaling overhead and power consumption during handover in LTE," in *IEEE Wireless Communications and Networking Conference (WCNC)*, 2019, pp. 1–6.

[17] N. Sinclair, D. Harle, I. A. Glover, and R. C. Atkinson, "A kernel methods approach to reducing handover occurrences within LTE," in *VDE 18th European Wireless Conference*, 2012, pp. 1–8.

[18] R. Arshad, H. Elsawy, S. Sorour, T. Y. Al-Naffouri, and M.-S. Alouini, "Handover management in 5G and beyond: A topology aware skipping approach," *IEEE Access*, vol. 4, pp. 9073–9081, 2016.

[19] H. Zhang, W. Ma, W. Li, W. Zheng, X. Wen, and C. Jiang, "Signalling cost evaluation of handover management schemes in LTE-advanced femtocell," in *IEEE 73rd Vehicular Technology Conference (VTC Spring)*, 2011, pp. 1–5.

[20] H. Zhang, W. Zheng, X. Wen, and C. Jiang, "Signalling overhead evaluation of HeNB mobility enhanced schemes in 3GPP LTE-Advanced," in *IEEE 73rd Vehicular Technology Conference (VTC Spring)*, 2011, pp. 1–5.

[21] M. Z. Chowdhury and Y. M. Jang, "Handover management in high-dense femtocellular networks," *EURASIP Journal on Wireless Communications and Networking*, no. 1, pp. 1–21, 2013.

[22] A. M. Vegni and T. D. Little, "Handover in VLC systems with cooperating mobile devices," in *IEEE International conference on computing, networking and communications (ICNC)*, 2012, pp. 126–130.

[23] E. Dinc, O. Ergul, and O. B. Akan, "Soft handover in OFDMA based visible light communication networks," in *IEEE 82nd Vehicular Technology Conference (VTC2015-Fall)*, 2015, pp. 1–5.

[24] M. S. Demir, F. Miramirkhani, and M. Uysal, "Handover in VLC networks with coordinated multipoint transmission," in *IEEE International Black Sea Conference on Communications and Networking (BlackSeaCom)*, 2017, pp. 1–5.

[25] F. Wang, Z. Wang, C. Qian, L. Dai, and Z. Yang, "Efficient vertical handover scheme for heterogeneous VLC-RF systems," *Journal of Optical Communications and Networking*, vol. 7, no. 12, pp. 1172–1180, 2015.

[26] Y. Wang and H. Haas, "Dynamic load balancing with handover in hybrid Li-Fi and Wi-Fi networks," *IEEE Journal of Lightwave Technology*, vol. 33, no. 22, pp. 4671–4682, 2015.

[27] Y. Wang, D. A. Basnayaka, X. Wu, and H. Haas, "Optimization of load balancing in hybrid LiFi/RF networks," *IEEE Transactions on Communications*, vol. 65, no. 4, pp. 1708–1720, 2017.

[28] X. Lin, R. K. Ganti, P. J. Fleming, and J. G. Andrews, "Towards understanding the fundamentals of mobility in cellular networks," *IEEE Trans. Wireless Commun.*, vol. 12, no. 4, pp. 1686–1698, 2013.

[29] W. Bao and B. Liang, "Stochastic geometric analysis of user mobility in heterogeneous wireless networks," *IEEE J. Sel. Areas Commun.*, vol. 33, no. 10, pp. 2212–2225, 2015.

[30] S. Sadr and R. Adve, "Handoff rate and coverage analysis in multi-tier heterogeneous networks," *IEEE Trans. Wireless Commun.*, vol. 14, no. 5, pp. 2626 – 2638, 2015.

[31] S.-Y. Hsueh and K.-H. Liu, "An equivalent analysis for handoff probability in heterogeneous cellular networks," *IEEE Communications Letters*, vol. 21, no. 6, pp. 1405–1408, 2017.

[32] X. Wu and H. Haas, "Handover skipping for LiFi," *IEEE Access*, vol. 7, pp. 38 369–38 378, 2019.

[33] M. Tayyab, X. Gelabert, and R. Jäntti, "A simulation study on handover in LTE ultra-small cell deployment: A 5G challenge," in *IEEE 2nd 5G World Forum (5GWF)*, 2019, pp. 388–392.

[34] M. Alhabo, L. Zhang, and N. Nawaz, "A trade-off between unnecessary handover and handover failure for heterogeneous networks," in *23th European Wireless Conference*, 2017, pp. 1–6.

[35] H. Tabassum, M. Salehi, and E. Hossain, "Fundamentals of mobility-aware performance characterization of cellular networks: A tutorial," *IEEE Communications Surveys & Tutorials*, vol. 21, no. 3, pp. 2288–2308, 2019.

[36] R. Arshad, H. ElSawy, L. Lampe, and M. J. Hossain, "Handover rate characterization in 3D ultra-dense heterogeneous networks," *IEEE Transactions on Vehicular Technology*, vol. 68, no. 10, pp. 10 340–10 345, 2019.

[37] M. D. Soltani, H. Kazemi, M. Safari, and H. Haas, "Handover modeling for indoor Li-Fi cellular networks: The effects of receiver mobility and rotation," in *IEEE Wireless Communications and Networking Conference (WCNC)*, 2017, pp. 1–6.

[38] J. G. Andrews, F. Baccelli, and R. K. Ganti, "A tractable approach to coverage and rate in cellular networks," *IEEE Trans. Commun.*, vol. 59, no. 11, pp. 3122–3134, 2011.

[39] C. Chen, D. A. Basnayaka, and H. Haas, "Downlink performance of optical attocell networks," *IEEE Journal of Lightwave Technology*, vol. 34, no. 1, pp. 137–156, 2015.

[40] H. Tabassum and E. Hossain, "Coverage and rate analysis for co-existing RF/VLC downlink cellular networks," *IEEE Transactions on Wireless Communications*, vol. 17, no. 4, pp. 2588–2601, 2018.

[41] C. Chen, D. Basnayaka, and H. Haas, "Downlink SINR statistics in OFDM-based optical attocell networks with a Poisson point process network model," in *IEEE Global Communications Conference (GLOBECOM)*, 2015, pp. 1–6.

[42] Chiu *et al.*, *Stochastic Geometry and its Applications*. John Wiley & Sons, 2013.

[43] A. K. Gupta and A. Banerjee, "On the spatial performance of users in indoor VLC networks with multiple reflections," in *IEEE International Conference on Signal Processing and Communications (SPCOM)*, 2018, pp. 512–516.

[44] P. F. Ash and E. D. Bolker, "Generalized dirichlet tessellations," *Geometriae Dedicata*, vol. 20, no. 2, pp. 209–243, 1986.

[45] J. Meinilä, P. Kyösti, T. Jämsä, and L. Hentilä, "Winner II channel models," *Radio Technologies and Concepts for IMT-Advanced*, pp. 39–92, 2009.

[46] J. Armstrong and B. J. Schmidt, "Comparison of asymmetrically clipped optical OFDM and DC-biased optical OFDM in AWGN," *IEEE Communications Letters*, vol. 12, no. 5, pp. 343–345, 2008.

[47] J. M. Kahn and J. R. Barry, "Wireless infrared communications," *Proceedings of the IEEE*, vol. 85, no. 2, pp. 265–298, 1997.

[48] X. Bao, X. Zhu, T. Song, and Y. Ou, "Protocol design and capacity analysis in hybrid network of visible light communication and OFDMA systems," *IEEE transactions on vehicular technology*, vol. 63, no. 4, pp. 1770–1778, 2013.

[49] Z. Li, S. Shao, A. Khreishah *et al.*, "Design and implementation of a hybrid RF-VLC system with bandwidth aggregation," in *IEEE 14th International Wireless Communications and Mobile Computing Conference (IWCMC)*, 2018, pp. 194–200.

[50] H.-S. Jo, Y. J. Sang, P. Xia, and J. G. Andrews, "Heterogeneous cellular networks with flexible cell association: A comprehensive downlink SINR analysis," *IEEE Trans. Wireless Commun.*, vol. 11, no. 10, pp. 3484–3495, 2012.

[51] M. Ding and D. L. Pérez, "Please lower small cell antenna heights in 5G," in *IEEE Global Communications Conference (GLOBECOM), Washington, DC*, 2016, pp. 1–6.

[52] Y. Ren, Y. Li, and C. Qi, "Handover rate analysis for k-tier heterogeneous cellular networks with general path-loss exponents," *IEEE Communications Letters*, vol. 21, no. 8, pp. 1863–1866, 2017.

[53] L. F. Shampine, "Vectorized adaptive quadrature in MATLAB," *Elsevier Journal of Computational and Applied Mathematics*, vol. 211, no. 2, pp. 131–140, 2008.